Clays and Clay Minerals, Vol. 57, No. 4, 465–475, 2009.

HIGH-RESOLUTION TRANSMISSION ELECTRON MICROSCOPY STUDY OF Fe-Mn OXIDES IN THE HYDROTHERMAL SEDIMENTS OF THE RED SEA DEEPS SYSTEM

NURIT TAITEL-GOLDMAN[1,*], VLADIMIR EZERSKY[2], AND DIMITRY MOGILYANSKI[3]

[1] The Open University of Israel, P.O. Box 808, Raanana, Israel
[2] Department of Material Engineering, Ben-Gurion University of the Negev, Beer-Sheva, Israel
[3] The Institutes for Applied Research, Ben-Gurion University of the Negev, Beer-Sheva, Israel

Abstract—Deep sediments from the Red Sea have been studied extensively and provide a rich resource for understanding mineral transformations under hydrothermal conditions. Interrelationships among various sampling sites, however, are still rather incomplete. The purpose of the present study was to increase understanding of these systems by characterizing and comparing the Fe-Mn oxyhydroxides from the southern Atlantis II, Chain A, Chain B, and Discovery Deeps, using high-resolution transmission electron microscopy. Some of the hydrothermal sediments of Chain A are dominated by Si-associated Fe oxides (ferrihydrite, goethite, lepidocrocite, and short-range ordered, rounded particles) resembling the hydrothermal sediments of the SW basin in the Atlantis II Deep, indicating sub-bottom connections between the Deeps. Although some of the sediments of the Discovery Deep show a similar trend; short-range ordered, rounded particles were not detected in these sediments, implying that crystallization of this short-range ordered phase is sensitive to the Si/Fe ratio in the brine and only at elevated ratios does it crystallize out of the brine. Silicon-associated and Fe-enriched Mn oxyhydroxides such as groutite, manganite, todorokite, and Mn-dominated lathlike layers occasionally contain Ca and Mg impurities. Manganese substitutes for Fe and *vice versa*, leading to a solid-solution series between goethite and groutite and Mn-enriched ferrihydrite. Hematite is the only Fe oxide in the hydrothermal sediments that is found to be lacking in impurities, which is probably due to its formation by recrystallization from other Fe oxides.

Key Words—Atlantis II System, Fe Oxides, Mn Oxides, Red Sea.

INTRODUCTION

The Atlantis II Deep system is located in the axial rift zone of the central Red Sea (21º15′N–21º27′N and 38º02′E–38º07′E) (Figure 1). Red Sea Deep Water (RSDW) that penetrates the sediments attains significant salinity by leaching Miocene evaporites and is heated along a geothermal gradient and interaction with hot basaltic rocks (Shankes and Bischoff, 1977; Cocherie *et al*., 1994). The hot brine that discharges into the southwest basin of the Atlantis II Deep creates a stratified brine system with a Lower Convecting Layer (LCL) enriched with Mn and Fe and an Upper Convecting Layer (UCL). During the last three decades of the 20th century the temperature of the LCL increased from 55.9ºC to 67.2ºC and that of the Upper Convecting Layer 1 (UCL1) from 44.3 to 56.3ºC, indicating an increase in hydrothermal activity (Scholten *et al.*, 2000, and references therein). The pH of the LCL brine is ~5.5 (Shanks and Bischoff, 1977). A narrow channel 2010 m deep connects the southern Atlantis II Deep and the three small basins of the Chain Deep (Chain A, B, and C Deeps) that are located south of the Atlantis II Deep. The Discovery Deep is situated ~5 km southwest of the southern part of the Atlantis II Deep and is separated by a sill at a depth of ~1990 m below sea level (Hartman *et al.*, 1998a, 1998b) (Figure 1). Hartman *et al.* (1998a) and Pierret *et al.* (2001) suggested that not only does the overflowing brine feed the adjacent deeps as suggested by Schoell and Hartmann (1973), but a fracture and fissure system enables a sub-bottom flow of the brine of the LCL from the Atlantis II Deep into the Chain and Discovery Deeps, leading to hydrothermal conditions in those deeps: Chain A 52.4–54ºC, Chain B 46ºC, Chain C 44.3ºC, and Discovery Deep 44.7ºC (Ramboz and Danis, 1990, Hartmann *et al.*, 1998b). The water salinity of the Chain A, B, C, and Discovery Deeps resembles that of the LCL of the Atlantis II Deep (Schoell and Faber, 1978, Hartmann *et al.*, 1998a), whereas pH values are slightly greater (pH 6.4) (Hartmann *et al.*, 1998a, Pierret *et al.*, 2001). The upper level of the main brine in the Discovery Deep resembles that of the LCL in the neighboring Atlantis II Deep (Hartmann, 1980; Hartmann *et al.*, 1998a). Elevated Fe and Mn concentrations were detected in the Atlantis II LCL (81 mg/kg for each element); reduced concentrations were detected in the Discovery Deep due to precipitation of Fe and Mn (Hartmann, 1985). At present, the most active area is the SW basin of the Atlantis II Deep as the sediments in this area are enriched with Fe. Manganese tends to precipitate more distally from the vent site (Scholten *et al.*, 2000).

* E-mail address of corresponding author:
nuritg@openu.ac.il
DOI: 10.1346/CCMN.2009.0570407

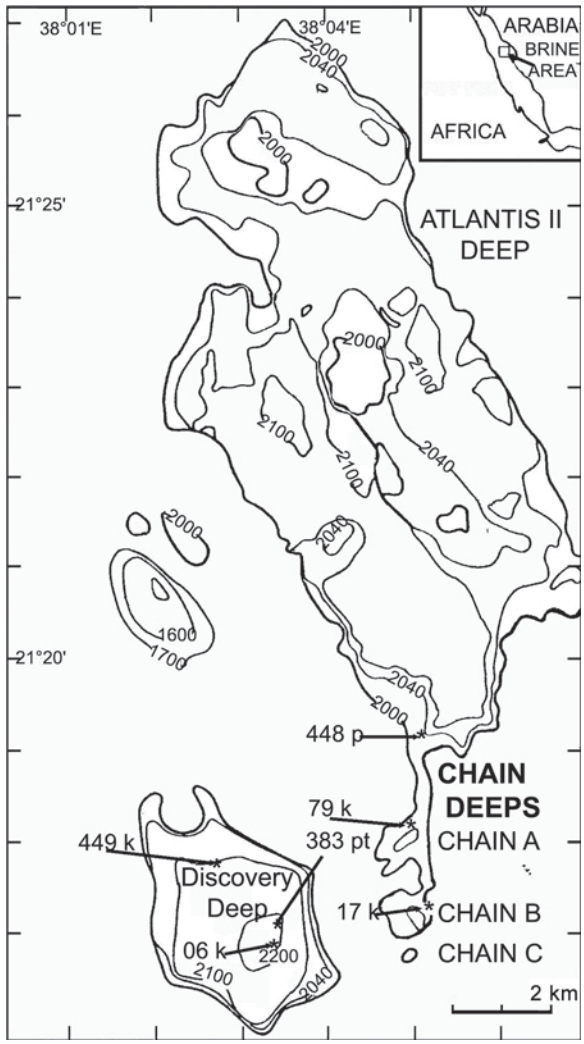

Figure 1. Map of the Atlantis II Deep system located in the Red Sea, with arrows indicating core sites (modified after Schoell and Hartmann, 1973).

The mineral assemblage of the Atlantis II Deep includes Mn-Fe carbonates (Taitel-Goldman *et al.*, 2008) and Si-associated Fe oxyhydroxides (short-range ordered, rounded particles: ferrihydrite, hematite, goethite, feroxyhyte, and lepidocrocite) which were found close to the sediment-brine interface and in the sedimentary column underneath (Taitel-Goldman and Singer 2001, 2002a; Taitel-Goldman *et al.*, 2002, 2004). Well crystallized Mn oxyhydroxides (manganite, todorokite, groutite, 10 Å buserite II, asbolane, and woodruffite) usually indicate marginal facies or ceasing of brine discharge for a long period (Bischoff, 1969; Butuzova and Lisitsyna, 1984; Butuzova *et al.*, 1990).

In the present work, a study of the Fe-Mn oxyhydroxides from the southern Atlantis II, Chain, and Discovery Deeps, mainly by high-resolution transmission electron microscopy (HRTEM), is presented.

METHODS

Samples from the Red Sea Deeps were collected from the vessel *R.V. Valdivia* during the Meseda 1st and 3rd cruises and the Sonne 02 and VA 29 cruises (for the Saudi-Sudanese Red Sea Joint Commission for Exploration of Red Sea Resources between 1977 and 1981). Samples from six cores from the southern part of the Atlantis II, Chain A, Chain B, and Discovery Deeps were studied (Table 1). The moist samples were stored at 4ºC from the time of their collection. Details of the treatment of the samples were described by Taitel-Goldman *et al.* (2002).

Transmission electron microscopy was carried out using a JEOL FasTEM 2010 electron microscope equipped with a Noran energy dispersive spectrometer (EDS) for microprobe elemental analyses. All chemical analyses were obtained by point analyses with a beam width of 25 nm and are presented as atomic ratios. A NORAN Standardless Metallurgical Thin Films program based on the Cliff-Lorimer ratio technique with an accuracy of ~5% was used for the calculations. The CuKα line was used to calibrate the spectrometer. Crystalline phases were identified using selected area electron diffraction (SAED) in the TEM. In this method a very high-energy electron beam (200 kV) transmits through the sample. The beam is diffracted at angles determined by Bragg's law, applied to a set of reflecting crystal planes separated by the *d* spacings of the crystals. In the case of amorphous or polycrystalline phases, the resultant diffraction pattern occurs as diffuse or partial rings. In the case of large crystals the pattern is geometric, reflecting the arrangement of crystals. Diffraction patterns can allow identification of *in situ* mineral phases with high accuracy and can differentiate between different minerals. The accuracy of the *d*-spacing determination was better than 0.005 nm. The smallest area of SAED was 100 nm. The 'dark field' (DF) technique was used to detect those particles which give diffraction spots: the direct beam was blocked by the aperture while one or more diffracted beams were allowed to pass the objective aperture. In the DF image some of the crystals appeared with strong contrast, *i.e.* those which diffracted into the aperture. To identify additional phases, powder X-ray diffraction (XRD) of un-oriented, oriented, and glycolated samples, using a Phillips 17130/1710 or Philips 1050 powder diffractometer, was performed. Infrared (IR) spectra were obtained using a Nicolet FTIR spectrometer (details given by Taitel-Goldman *et al.*, 2002).

RESULTS

Samples were collected from six cores: three from the southern part of the Atlantis II, Chain A, and Chain B Deeps and three from the Discovery Deep. The water depth varies between 2000 m in the Chain B Deep core

Table 1. Sampling locations.

Sample No.	Deep	Core No.	Position	Water depth below sea level (m)	Sample depth (m)
GN 280	Chain A	VA29 079KS	21°18.8N 38°05.2E	2033	0.10
GN 281	Chain A	VA29 079KS			0.40
GN 282	Chain A	VA29 079KS			0.85
GN 283	Chain A	VA29 079KS			1.30
GN 284	Chain A	VA29 079KS			1.73
GN 323	Chain B	VA01 17K	21°17′13″N 38°05′08″E	2000	0.30
GN 324	Chain B	VA01 17K			1.47
GN 285	Discovery	SO-02 449K	21°17.42′N 38°02.84′E	2176	0.35
GN 286	Discovery	SO-02 449K			0.70
GN 287	Discovery	SO-02 449K			0.97
GN 288	Discovery	SO-02 449K			1.16
GN 289	Discovery	SO-02 449K			1.79
GN 319	Discovery	VA01 06K	21°16′48″N 38°03′13″E	2208	0.57
GN 320	Discovery	VA01 06K			0.90
GN 321	Discovery	VA01 06K			1.24
GN 322	Discovery	VA01 06K			1.80
GN 325	NE Discovery	VA03 383PTT	21°17.00′N 38°05′08″E	2216	2.18
GN 326	NE Discovery	VA03 383PTT			2.37
GN 327	NE Discovery	VA03 383PTT			2.57
GN 328	NE Discovery	VA03 383PTT			2.78
GN 290	Southern Atlantis II Deep	SO 02 448P	21°17.17′N 38°04.85′E	2073	0.10
GN 291	Southern Atlantis II Deep	SO 02 448P			0.35

to 2216 m below sea level for the cores collected from the Discovery Deep.

Southern Atlantis II Deep

Two samples that were collected from the southern part of the Atlantis II Deep *via* Chain A Deep contain mainly biogenic and terrigenous materials such as calcite and smectite. Iron oxides appear in three forms: well crystallized hematite (α-Fe_2O_3), goethite (α-FeOOH), and clusters of ferrihydrite ($Fe_5^{3+}HO_8{\cdot}4H_2O$). Hematite crystals are free of impurities, whereas the ferrihydrite composition includes Si and Mn impurities (Si/Fe – 0.12 and Mn/Fe – 0.16) (Figure 2a,b). High-resolution images of ferrihydrite show tiny, short-range ordered crystallites <5 nm in size (Figure 2c). Si-associated goethite needles, up to 200 nm long (Si/Fe – 0.04), have Mn/Fe ratios of 0.1 (Figure 2d).

Manganese oxides include todorokite ($(Ca,Mg)_{1-x}Mn^{4+}O_{12}{*}3{-}4H_2O$), groutite ($\alpha$-$Mn^{3+}OOH$), manganite ($\gamma$Mn OOH), and thin, curved, folded layers of Mn oxyhydroxides. Todorokite appears as 500 nm subhedral plates with noticeable cleavage (Figure 3a). Chemical analyses yielded additional Si, Fe, Ca, and Mg reaching ratios for Si/Mn of 0.15; Fe/Mn 0.60; Ca/Mn 0.09; and Mg/Mn 0.03. Crystalline groutite (Figure 3b) appears as elongate mono-domain, platy, or prismatic needles that vary in size from 100 nm to >10 μm. Groutite crystals are frequently covered with tiny goethite crystals of 20–30 nm (Figure 3c). Tiny fibrous crystals of manganite have Fe and Si impurities of Fe/Mn – 0.2 and Si/Mn – 0.1 (Figure 3d). From high-resolution images, *d* spacings of 0.48 nm were obtained (Figure 3e). Another Mn oxyhydroxide phase that appears as curved and folded thin layers (~10 nm) includes varying amounts of Fe impurities reaching ratios for Fe/Mn of 0.28 and Si impurities that reach a ratio of 0.36. Some of the point analyses yielded no additional ions, *i.e.* they were pure Mn oxyhydroxide phases, and in others, some Ca and Mg were present, reaching ratios for Ca/Mn of 0.08 and for Mg/Mn of 0.09 (Figure 3f,g). Smectite was detected having an Al/Si ratio of 0.35, Fe/Si of 0.25, and Mn/Si of 0.1.

Chain A Deep

Five samples were collected from a core in Chain A Deep. All of the samples studied contained Fe and Mn oxyhydroxides along with some clays and biogenic calcite and aragonite. Manganese oxyhydroxides included todorokite with Fe and Si impurities reaching ratios for Si/Mn of 0.08 and for Fe/Mn of 0.15 (Figure 4a,b). Usually, ferrihydrite has additional Si reaching a ratio for Si/Fe of 0.31 (Figure 4c,d). Occasionally, Mn was also present, reaching ratios for Mn/Fe of 0.20 (Figure 4b). Another common phase in the Chain A Deep is mono-domain goethite, having Si/Fe ratios of 0.17 (Figure 5a–c). A third Fe-rich phase that was initially described from the Atlantis II Deep hydrothermal sediments is a short-range ordered phase having a morphology of rounded particles with an outer rim forming an electron-dense (thicker, more ordered)

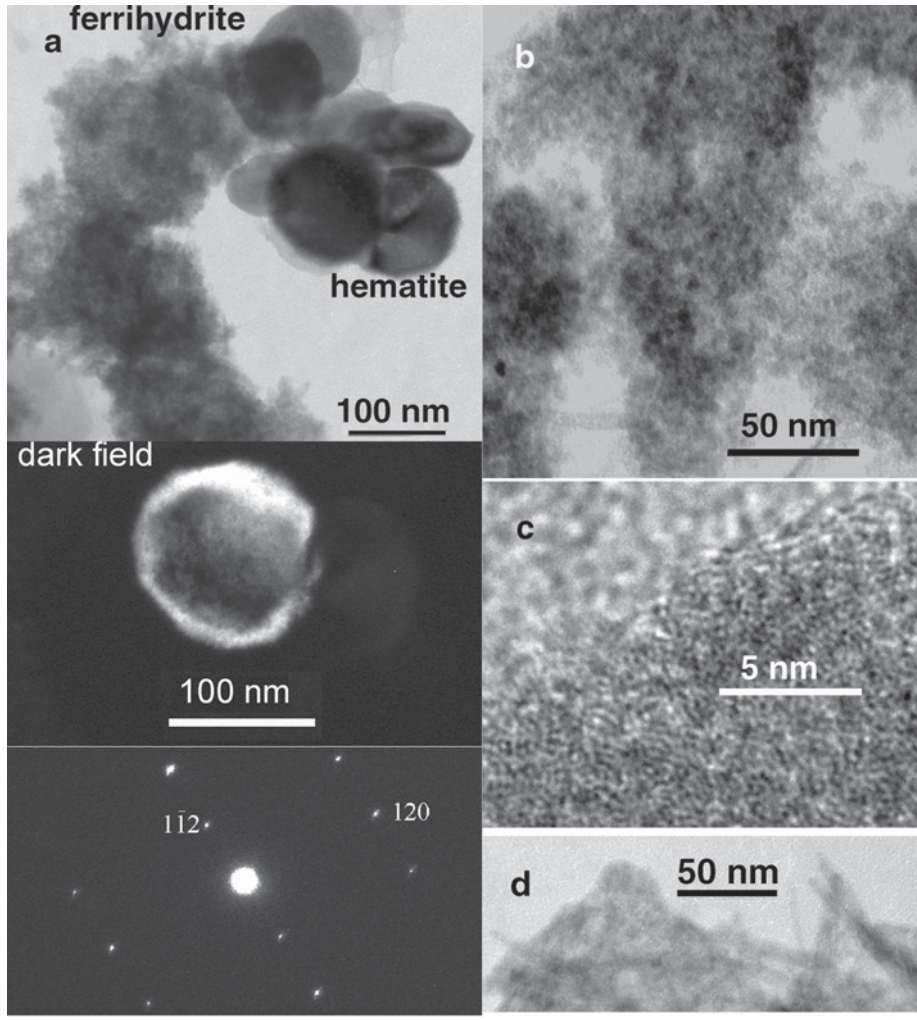

Figure 2. Images of Fe and Mn oxyhydroxides from the southern part of Atlantis II Deep: (a) well crystallized hematite and clusters of ferrihydrite with ratios for Si/Fe of 0.12 and Mn/Fe of 0.16, in the lower part of the SAED image of the hematite particle along with the DF image, indicating the diffraction source; (b) ferrihydrite clusters; (c) high-resolution image of ferrihydrite; (d) goethite with a Si/Fe ratio of 0.04 and a Mn/Fe ratio of 0.10.

ring, and an inner layer of fine-grained material. According to Taitel-Goldman and Singer (2002b), these rounded particles have a disc morphology with a polycrystalline core and a composition of $(SiFe_4O_6(OH)_4.H_2O)$. Due to the short-range ordered structure, this phase cannot be classified as a mineral but as a mineraloid. Some of the particles appear to have disintegrated and to have re-crystallized into a clay, namely nontronite (Figure 5a).

Chain B Deep

Two samples were collected from a core in the Chain B Deep. In both samples, ferrihydrite is a common Fe hydroxide, with additional Si and Mn reaching ratios for Si/Fe of 0.33 and for Mn/Fe of 0.24 (Figure 6a,b). Multi-domain Si-associated goethite (Si/Fe – 0.24) forms crystals up to ~200 nm in size (Figure 6b). Iron-rich manganite (ratio of Fe/Mn up to 0.79) (Figure 6c), Si-associated groutite (Si/Mn – 0.14) (Figure 6d), and thin layers of Mn oxyhydroxides (ratio of Si/Mn up to 0.37, Fe/Mn – 0.24) comprise the Mn oxyhydroxide assemblage in the samples studied.

Discovery Deep

Three cores from the Discovery Deep were studied: SO-02 449K, VA01 06K, and VA03 383PT. Apart from biogenic debris and some clays, various well crystallized Fe oxides appear in all the samples studied. Si-associated mono-domain and multi-domain goethite (Figure 7a), Si-associated lepidocrocite (Figure 7b,c), and pure hematite (Figure 7d) were found in cores SO-02 449K and in VA01 06K. The Si/Fe ratios in goethite vary between pure mono-domain goethite to 0.34 in core SO-02 449K and reach almost 0.50 in Core

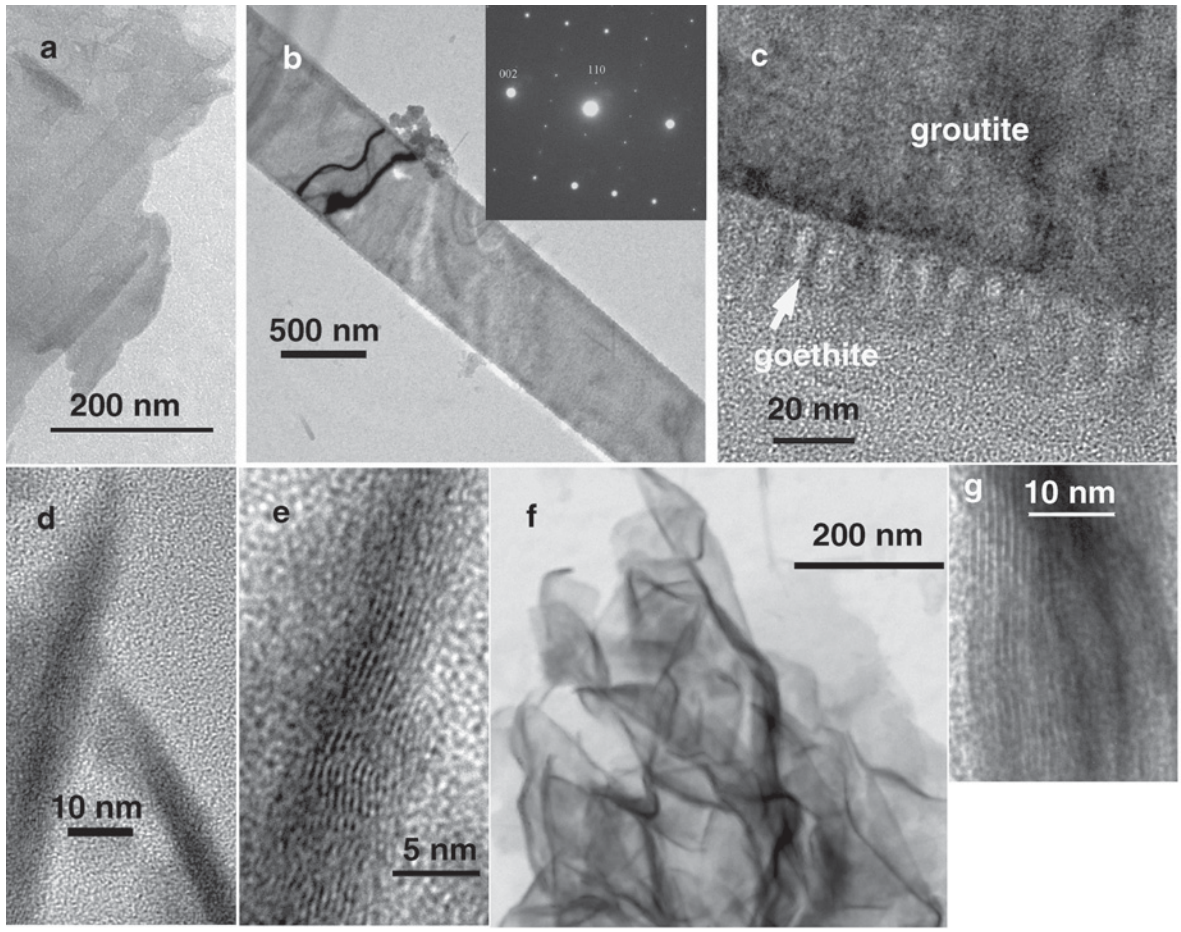

Figure 3. Mn oxyhydroxides from the Atlantis II Deep: (a) platy crystals of todorokite with ratios for Si/Mn of 0.15, Ca/Mn of 0.09, and Fe/Mn of 0.28; (b) large groutite crystal with a SAED image showing the diffraction pattern; (c) high-resolution image of a groutite crystal with tiny goethite crystals on the groutite surface; (d) two manganite needles with ratios for Fe/Mn of 0.2 and Si/Mn of 0.1; (e) high-resolution image of the manganite crystal in the left of part d with a distance between the layers of 0.48 nm; (f) Mn oxyhydroxide layers having ratios for Si/Mn of 0.09, Fe/Mn of 0.10, Ca/Mn of 0.03, and Mg/Mn of 0.04; (g) high-resolution image of a Mn oxyhydroxide layer; the *d* spacing calculated from the image, using fast Fourier transform, yielded 0.484 and 0.248 nm.

VA01 06K. Similarly, lepidocrocite is platy, with Si/Fe ratios that vary between 0.05 and 0.33 in core SO-02 449K and reach a ratio of 0.5 in core VA01 06K. Tiny hematite crystals appear only in core SO-02 449K without any impurities. Samples collected from core VA03 383PT differ in their mineral assemblage because Mn is present in all phases. A goethite-groutite phase (ratio of Mn/Fe up to 0.8 and Si/Fe of 0.3) is present along with manganite that has elongate crystals forming a large cluster and having Si impurities that reach a ratio for Si/Mn of 0.09 (Figure 7e). Folded, thin layers of Mn-Fe oxyhydroxides appear in samples from the VA03 383PT core. Si/Fe ratios of 0.24 and for Mn/Fe of 0.25 characterize these layers (Figure 7f). Their inner structure appears as a short-range ordered phase consisting of a few layers only. Mn-rich ferrihydrite clusters are also common in this core, having a Mn/Fe ratio of 0.13 and a Si/Fe ratio of 0.34 (Figure 7h).

Silicon affects the crystal size of both the Fe and Mn oxides (Figure 8a,b). The largest crystals of groutite apparently include small amounts of Si, whereas in manganite the Si/Mn ratio is greatest in the smallest crystals. Groutite has the smallest Si/Mn ratio, *i.e.* 0.03, in the Atlantis II Deep and 0.05 in Chain B. The todorokite Si/Mn ratio varies from a pure phase in the Discovery Deep to 0.12 in the southern Atlantis II Deep. Tiny fibrous manganite crystals, found in samples from the southern Atlantis II and Chain B Deeps, are Si-associated, with Si/Mn values ranging between 0.10 and 0.20. A similar trend was observed in Fe oxides, both goethite and lepidocrocite. Ferrihydrite crystals of all the samples studied have the smallest crystal size and elevated Si/Fe ratios.

Comparison of IR spectra of the bulk samples studied and of the XRD patterns shows that in some clay-free samples a peak at ~1000–1007 cm^{-1} was observed.

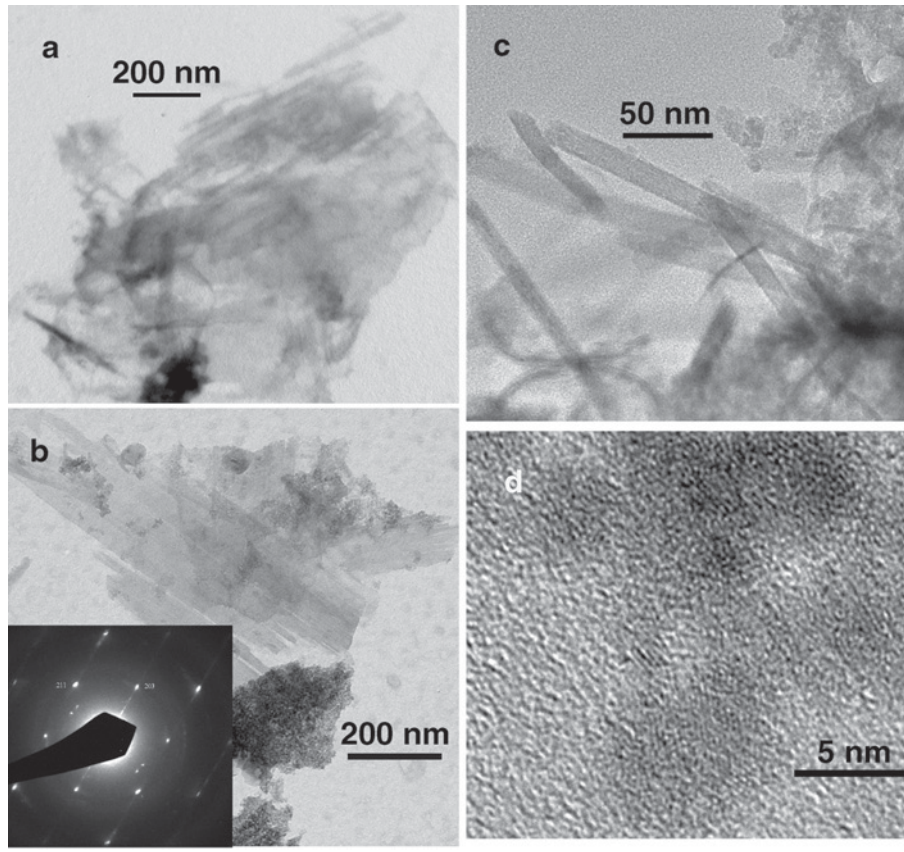

Figure 4. Images of samples from the Chain A Deep: (a) multi-domain todorokite with ratios for Si/Mn of 0.06 and Fe/Mn of 0.15. The individual dark crystal on the left has ratios for Si/Mn of 0.08 and Fe/Mn of 0.13; (b) todorokite multi-domain prismatic crystals with a ratio for Fe/Mn of 0.08 and a ferrihydrite cluster with ratios for Si/Fe of 0.31 and Mn/Fe of 0.12; (c) goethite has a ratio for Si/Fe of 0.15, whereas ferrihydrite yielded a Si/Fe ratio of 0.29; (d) high-resolution image of ferrihydrite.

DISCUSSION

Precipitation of Fe-Mn phases characterizes the authigenic mineral assemblage of the marginal facies in the Atlantis II system and the adjacent Deeps. The similarity between the ion size of Mn^{3+} and Fe^{3+} leads to their mutual substitution. Most of the Fe oxides have Mn impurities and Mn oxides usually contain varying amounts of Fe. Few samples differ by having goethite, lepidocrocite, and ferrihydrite without any Mn impurities, suggesting that they crystallized from brine similar to that of the LCL of the Atlantis II Deep and not in marginal facies. As suggested by Hartman *et al.* (1998a) and Pierret *et al.* (2001), the brine of the lower convecting layer of the Atlantis II Deep flows into the neighboring Deeps through a fissure and fracture system. Iron oxides that precipitated from that brine lack Mn impurities and were found only in the deeper sediments of the Chain A Deep and Discovery Deep. Intensified brine discharge in the Atlantis II Deep that could level up the LCL-UCL1 interface leading to overflow of the lower-most brine into neighboring Deeps cannot be ruled out.

Marginal facies as observed mainly in shallower samples include Fe and Mn phases or mixed Fe-Mn phases. At these shallower depths, the brine resembles that of the UCL1 or the Transition Zone to Red Sea Deep Water (RSDW). Elevated pH and Mn concentrations along with some oxygen from the overlying RSDW enables precipitation of Mn oxyhydroxides (Hartmann, 1985). The Mn phases are well preserved and not dissolved, as they were deposited at marginal facies away from the LCL that is characterized by a lower pH. Usually, at the LCL, Mn oxides dissolve and Fe oxides are formed instead using the dissolved oxygen (Scholten *et al.*, 2000, and references therein). At shallower water depth, not only did Mn phases precipitate but also Fe oxides with elevated Mn concentrations.

The co-precipitation of Mn goethite has been well documented, in both experimental studies and natural samples (Scheinost *et al.*, 2001; Wells *et al.*, 2006). Incorporation of Mn into the goethite structure causes a shift in the unit-cell parameters toward those of groutite (Ebinger and Schulze, 1990); incorporation of Fe into groutite crystals showed that both reflect a solid-solution of goethite-groutite end members (Ebinger and Schulze, 1989). According to Wells *et al.* (2006), incorporation of Mn into goethite does not form groutite clustering within

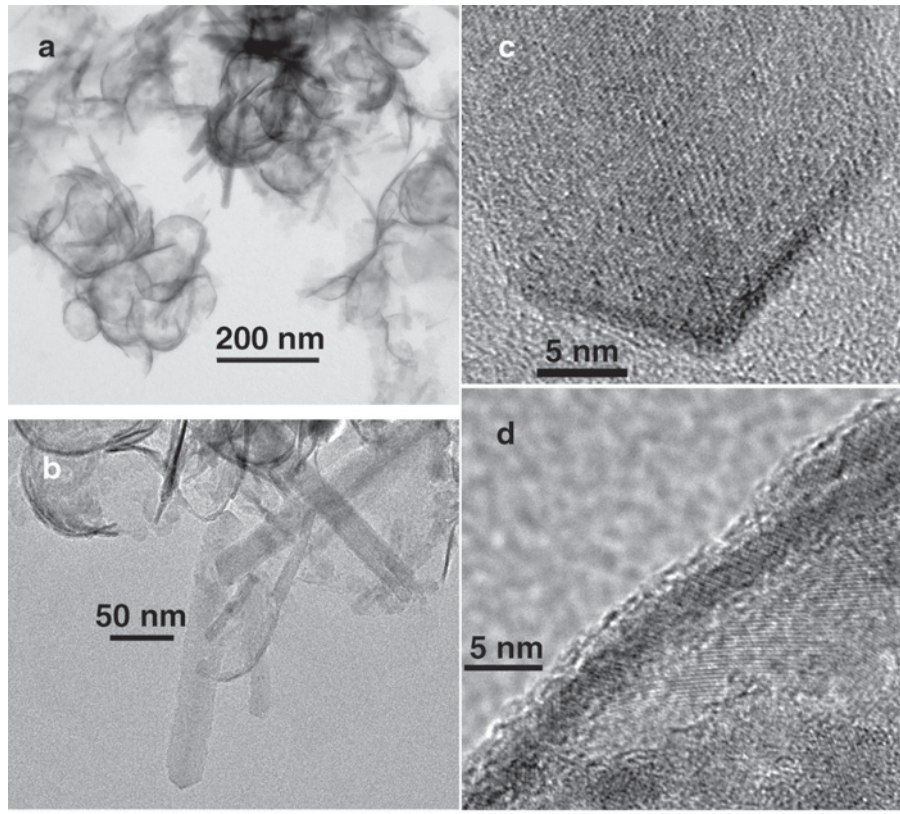

Figure 5. Well crystallized goethite and Si-Fe short-range ordered, rounded particles from Chain A Deep: (a) short-range ordered, rounded particles with a Si/Fe ratio of 0.22; (b) tiny ferrihydrite crystals, short-range, rounded particles, and well crystallized goethite; (c) high-resolution image of well crystallized, mono-domain goethite; (d) high-resolution image of short-range, rounded particles showing outer electron-dense rims and inner short-range ordered structure.

the goethite crystals but Mn^{3+} incorporated into the goethite structure, having an inhomogeneous distribution (Sileo *et al.*, 2001). The ratio of substitution measured in laboratory experiments was small and such substitutions in natural samples were rare (Scheinost *et al.*, 2001, and references therein); yet, at pH 6 and 50ºC, elevated Fe/Mn ratios apparently were obtained in Mn goethite synthesis (Ebinger and Schulze, 1990) and in Fe groutite (Ebinger and Schulze, 1989). These experimental conditions agree quite well with those prevailing in the marginal facies of the Atlantis II Deep system and the adjacent Deeps, thus enabling the co-precipitation of Fe-rich groutite and Mn-rich goethite. As for ferrihydrite, Fe substitution by Mn was obtained mainly through synthesis under alkaline conditions (Giovanoli and Cornell, 1992).

Overall, samples from the marginal facies of the Atlantis II Deep and the adjacent Deeps exhibit a charactereristic imprint. Apart from pure hematite, which results from re-crystallization of a former phase, all Fe and Mn oxyhydroxides are Si-associated. Si-associated goethite and lepidocrocite were described in the sediments of the Atlantis II Deep resulting from the Si-enriched brine that discharges into the deep (Taitel-Goldman *et al.* 2002, 2004). The unit-cell parameters of goethite and lepidocrocite did not change, however, so Si evidently does not substitute for Fe, but it does hinder particle growth (Taitel-Goldman and Singer, 2002). A similar trend was observed in goethite and lepidocrocite crystals presented in the present study, *i.e.* no significant change in unit-cell parameters was observed in either phase, yet their crystal size was affected. Ferrihydrite differs from other Fe oxides in having elevated Si/Fe ratios and the smallest crystal size. Infrared data obtained in this study (peak at ~1000) comply with the possible Fe-O-Si linkage in ferrihydrite in clay-free samples (Cornell and Schwertmann, 2003, and references therein). Not only are the Fe oxides Si-associated, but a similar association also exists within Mn oxides. Apparently, Si also affects growth of the Mn phase. The largest groutite crystals have the smallest Si/Mn ratios, whereas some manganite crystals which are very small have the greatest Si/Mn ratios.

As Si was found to hinder crystal growth of Fe and Mn oxides, elevated Si concentrations led to precipitation of short-range ordered phases. Elevated Si concentrations in ferrihydrite from the Atlantis II Deep sediments were described by Taitel-Goldman and

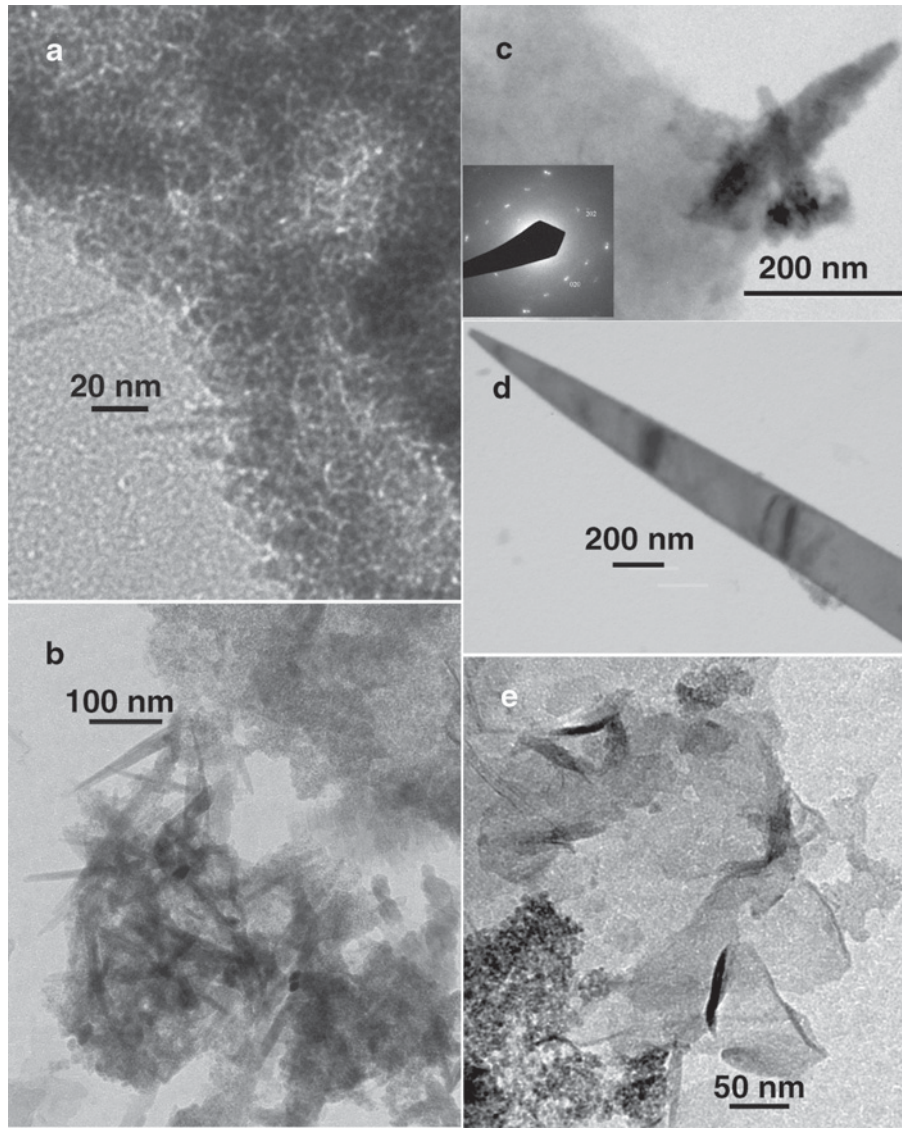

Figure 6. Images of Fe and Mn oxyhydroxide from the Chain B Deep: (a) cluster of ferrihydrite; (b) cluster of ferrihydrite particles with multi-domain Si-associated goethite with a Si/Fe ratio of 0.24; (c) two elongate manganite crystals with Fe/Mn ratios of 0.53–0.79, Si/Mn ratios of 0.14–0.2, and a silicate particle with ratios for Fe/Si of 0.13 and K/Si of 0.05; the SAED pattern was obtained from the upper needle; (d) groutite crystal with ratios for Si/Mn of 0.05 and for Mg/Mn of 0.05; (e) ferrihydrite with a Si/Fe ratio of 0.22 and Mn oxyhydroxide folded layers with a Si/Mn ratio of 0.37.

Singer (2001). In the present study, apart from Si enrichment in ferrihydrite, Mn was also found as an impurity in ferrihydrite samples, implying that Mn might substitute for Fe in ferrihydrite. Another phase that was described in previous studies of the sediments from the Atlantis II Deep is a short-range ordered phase which has disc morphology with an electron-dense outer rim. Synthesis of this phase showed that it crystallized from brines characterized by elevated Si/Fe ratios (Si/Fe 1.5) and that it eventually transformed by recrystallization into nontronite (Taitel-Goldman and Singer, 2002). In the present study, this phase was detected only in samples from Chain A Deep and some of the particles seemed to disintegrate and re-crystallize into nontronite (Figure 5). Only in Chain A Deep could the amount of Si available support the crystallization of these Si-Fe rounded particles. Away from the discharging brine, some of the Si was consumed by other phases, the Si/Fe ratio in the brine was reduced, and crystallization of the Si-Fe round particles ceased.

Thin layers which consist mainly of Mn oxyhydroxides and seldom of Fe oxyhydroxides exhibited a curved and folded morphology. Among the Mn-dominated phases, the amount of impurities varies between a

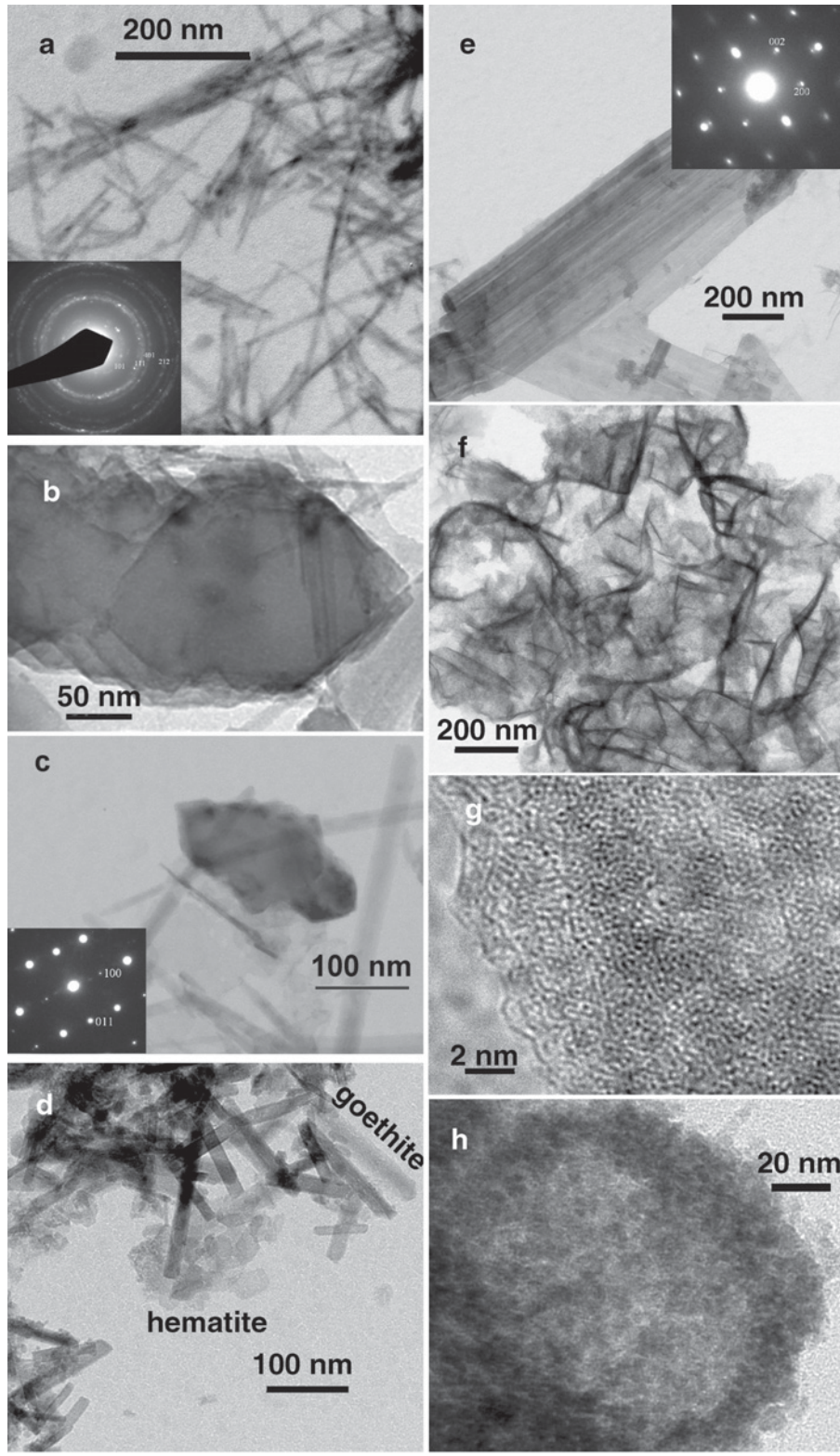

Figure 7. Images of samples from the Discovery Deep: (a) mono-domain and multi-domain goethite crystals; (b) lepidocrocite crystals with lath-like morphology; (c) lepidocrocite together with elongate mono-domain goethite; (d) small hematite crystals among elongate goethite crystals; (e) manganite crystals; (f) folded, thin layers of an oxyhydroxide similar to feroxyhyte with ratios for Si/Fe of 0.24, for Mn/Fe of 0.25; (g) high-resolution image of a Si-Fe-Mn oxide; (h) rounded cluster of ferrihydrite.

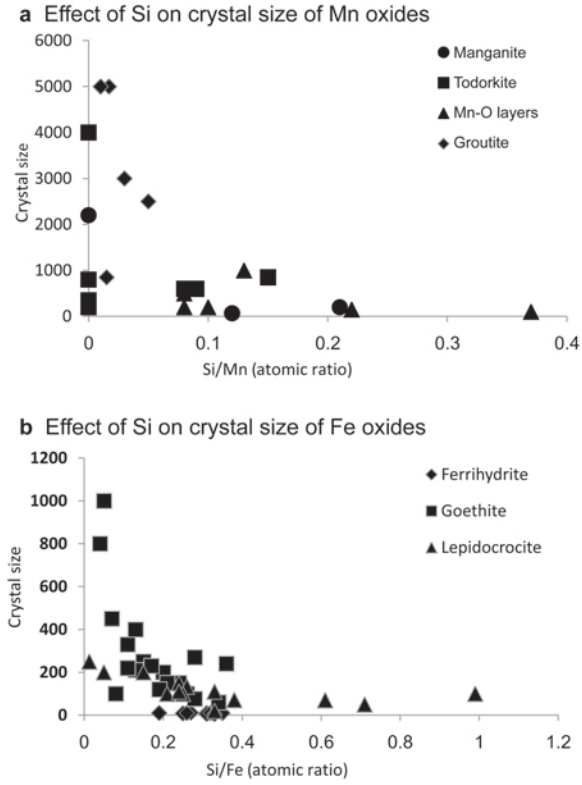

Figure 8. Effect of Si on the crystal size of Mn and Fe oxides. Measurements were obtained by point analyses and the crystal sizes measured from the TEM images.

pure Mn oxyhydroxide to others which contain some Fe, Si, Ca, and Mg, reaching the following ratios: Fe/Mn 0.31, Si/Mn 0.37, Ca/Mn 0.08, and Mg/Mn 0.08. An Fe-dominated short-range ordered layered phase was found in the Discovery Deep only, with elevated Si and Mn impurities (ratios for Si/Fe of 0.24 and for Mn/Fe of 0.25). Although the Mn end member resembles buserite ($Na_4Mn_{14}O_{27}$*$21H_2O$) or asbolane $(Ni,Co)_{2-x}Mn(O,OH)_4$*nH_2O, essential elements such as Na, Ni, and Co are lacking. The phase containing Fe-dominated layers differs in its morphology and size from short-range ordered rounded particles but resembles that of feroxyhyte (δFeOOH) described from the Atlantis II Deep (Taitel-Goldman and Singer, 2001). The Mn-Fe layered phases are actually one phase made of a solid-solution of Fe and Mn oxyhydroxides. The associated Si seems to hinder crystal growth of this phase also, leading to a short-range ordered phase.

CONCLUSIONS

(1) Hydrothermal sediments in the southern Atlantis II Deep and in the adjacent Chain and Discovery Deeps resemble those described from the Atlantis II Deep: a lepidocrocite-goethite association which crystallizes out of the hydrothermal brine contains no Mn impurities, indicating precipitation from hot hydrothermal brine and not at marginal facies. The presence of Mn phases, on the other hand, indicates precipitation from UCL or even from the transition zone to RSDW. Short-range ordered, rounded particles were found only in the Chain A Deep sediments. Their absence in other Deeps indicates that the Si/Fe ratios in these Deeps were smaller as Si was previously consumed by other phases.

(2) Silicon that discharges into the Atlantis II Deep brine system precipitates mainly in association with Fe and Mn authigenic phases and seldom as amorphous pure silicate phases. Hence, Fe and Mn phases are the main sink for removal of Si from the brine.

(3) A short-range ordered Mn-Fe solid-solution of oxyhydroxides with thin, curved, and folded layers was discovered. The phases resemble the feroxyhyte structure rather than asbolane, as essential impurities needed for definition were not detected. Further study of these oxyhydroxides is needed to understand their structure better.

ACKNOWLEDGMENTS

The authors acknowledge The Open University of Israel Research Fund for financial support of this research. The IFM-GEOMAR Institute, Kiel, Germany, and Prof. P. Stoffers of the Institute for Geosciences, University of Kiel, are gratefully acknowledged for supplying the samples. The authors thank Prof. Arieh Singer, of the Hebrew University of Jerusalem, for his comments, and Associate Editor, Helge Stanjek, and two anonymous reviewers for their constructive reviews, which greatly improved the manuscript.

REFERENCES

Bischoff, J.L. (1969) Red Sea geothermal brine deposits: their mineralogy, chemistry and genesis. Pp. 368–401 in: *Hot Brines and Recent Metal Deposits in the Red Sea* (E.T. Degens and D.A. Ross, editors). Springer Verlag, Berlin, Heidelberg, New York.

Butuzova, G.Yu. and Lisitsyna, N.A. (1984) Metal deposits in deep subbasins of the Red Sea: Ore geochemistry and distribution pattern. *Lithology and Minerals Resources USSR*, **18**, 224–238.

Butuzova, G.Yu., Drtitz, V.A., Morozov, A.A. and Gorschkov, A.I. (1990) Processes of formation of iron-manganese oxyhydroxides in the Atlantis II and Thetis Deeps of the Red Sea. *Special Publication of the International Association of Sedimentologists*, **11**, 57–72.

Cocherie, A., Calvez, J.Y., and Oudin-Dunlop, E. (1994) Hydrothermal activity as recorded by Red Sea sediments: Sr-Nd isotopes and REE signatures. *Marine Geology*, **118**, 291–302.

Cornell, R.M. and Schwertmann, U. (2003) *The Iron Oxides: Structure, Properties, Reactions, Occurrences*. Wiley VCH, Weinheim, Germany

Ebinger, M.H. and Schulze, D.G. (1989) Mn substituted goethite and Fe substituted groutite synthesized at acid pH. *Clays and Clay Minerals*, **37**, 151–156.

Ebinger, M.H. and Schulze, D.G. (1990) The influence of pH on the synthesis of mixed Fe-Mn oxide minerals. *Clay Minerals*, **25**, 507–518.

Giovanoli, R. and Cornell, R.M. (1992) Crystallization of metal substituted ferrihydrite. *Zeitschrift für*

Pflanzenernährung und Bodenkunde, **155**, 455–460.

Hartmann, M. (1980) Atlantis II Deep Geothermal brine system. Hydrographic situation in 1977 and changes since 1965 (Note). *Deep Sea Research*, **27A**, 161–171.

Hartmann, M. (1985) Atlantis II Deep Geothermal brine system. Chemical processes between hydrothermal brine and Red Sea deep water. *Marine Geology*, **64**, 157–177.

Hartmann, M., Scholten, J.C., Stoffers, P., and Wehner, F., (1998a) Hydrographic structure of brine filled deeps in the Red Sea – new results from Shaban, Kerbit, Atlantis II and Discovery Deep. *Marine Geology*, **144**, 311–330.

Hartmann, M., Scholten, J.C. and Stoffers, P. (1998b) Hydrographic structure of brine filled deeps in the Red Sea: correction of Atlantis II Deep temperatures. *Marine Geology*, **144**, 331–332.

Pierret, M.C., Clauer, N., Bosch, D. Blanc, C., and France-Lanord, C. (2001) Chemical and isotopic ($^{87}Sr/^{86}Sr$, $\delta^{18}O$, δD) constraints in the formation processes of Red Sea brines. *Geochimica et Cosmochimica Acta*, **65**, 1259–1275.

Ramboz, C. and Danis, M. (1990) Superheating in the Red Sea? The heat-mass balance of the Atlantis II Deep revisited. *Earth and Planetary Science Letters*, **97**, 190–210.

Scheinost, A.C., Stanjek, H., Schulze, D.G., Gasser, U., and Sparks, D.L. (2001) Structural environment and oxidation state of Mn in goethite-groutite solid-solutions. *American Mineralogist*, **86** 139–146.

Schoell, M. and Faber, E. (1978) New isotopic evidence for the origin of Red Sea brines. *Nature*, **275**, 436–438.

Schoell, M. and Hartmann, M. (1973) Detailed temperature structure of the hot brines in the Atlantis II Deep area (Red Sea). *Marine Geology*, **14**, 1–14.

Scholten, J.C., Stoffers, P., Garbe-Schönberg, D., and Moammar, M. (2000) Hydrothermal mineralization in the Red Sea. Pp. 369–395 in: *Handbook of Marine Mineral Deposits* (D.S. Cronan, editor). CRC Press, Boca Raton, Florida, USA.

Shanks, W.C. and Bischoff, J.L. (1977) Ore transport and deposition in the Red Sea geothermal system: a geochemical model. *Geochimica et Cosmochimica Acta*, **41**, 1507–1519.

Sileo, E.E. Alvarez, M., and Rueda, E.H. (2001) Structural studies on the manganese for iron substitution in the goethite-jacobsite system. *International Journal of Inorganic Materials*, **3**, 271–279.

Taitel-Goldman, N. and Singer, A. (2001) High-Resolution Transmission Electron microscopy study of newly formed sediments in the Atlantis II Deep, Red Sea. *Clays and Clay Minerals*, **49**, 174–182.

Taitel-Goldman, N. and Singer, A. (2002a) Synthesis of clay-sized iron oxides under marine hydrothermal conditions. *Clay Minerals*, **37**, 719–731.

Taitel-Goldman, N. and Singer, A. (2002b) Metastable Si-Fe phases in hydrothermal sediments of Atlantis II Deep, Red Sea. *Clay Minerals*, **37**, 235–248.

Taitel-Goldman, N., Bender-Koch, C., and Singer, A. (2002) Lepidocrocite in hydrothermal sediments of the Atlantis II and Thetis Deeps, Red Sea. *Clays and Clay Minerals*, **50**, 186–197.

Taitel-Goldman, N., Bender-Koch, C., and Singer, A. (2004) Si associated goethite in hydrothermal sediments of the Atlantis II and Thetis Deeps, Red Sea. *Clays and Clay Minerals*, **52**, 115–129.

Taitel-Goldman, N., Ezersky V., and Mogilyanski, D. (2008) Study of Mn-siderite-rhodochrosite from the hydrothermal sediments of the Atlantis II Deep, Red Sea. *Israel Journal of Earth Sciences*, **57**, 45–54.

Wells, M.A., Fitzpatrick, R.W., and Gilkes, R.J. (2006) Thermal and mineral properties of Al^{-}, Cr^{-}, Mn^{-}, Ni^{-}, and Ti-substituted goethite. *Clays and Clay Minerals*, **54**, 176–194.

(*Received 25 November 2008; revised 1 July 2009; Ms. 0237; A.E. D.C. Bain*)